Materials Science Forum Vols. 539-543 (2007) pp. 3407-3413
online at http://www.scientific.net
© (2007) Trans Tech Publications, Switzerland

Twinning and Detwinning During Cyclic Deformation of Mg Alloy AZ31B

D. W. Brown[1, a], A. Jain[2, b], S. R. Agnew[2, c], and B. Clausen[1,d]

[1]MS-H805, BLDG 622, TA-53, Los Alamos National Laboratory, Los Alamos, NM 87545, USA

[2]Department of Materials Science and Engineering, University of Virginia, Charlottesville, VA 22904, USA

[a]dbrown@lanl.gov, [b]ashu@virginia.edu, [c]agnew@virginia.edu, [d]clausen@lanl.gov

Keywords: Cyclic loading; Deformation twin; Neutron diffraction; Internal strain; Magnesium; hcp.

Abstract. Textured Mg alloys exhibit tension – compression strength asymmetry due to mechanical twinning. The distinction arises as the material deforms primarily by slip in one direction and by twinning in the other. In-situ neutron diffraction during cyclic loading in tension and compression of extruded bar allows study of the effect of twinning on subsequent load reversals. The diffraction data reveal the texture evolution and internal stress development as a function of deformation. De-twinning resulted in complete texture reversal during initial cycles, but eventually "fatigued" resulting in some residual twin component.

Introduction

Secondary deformation mechanisms such as deformation twinning are particularly important for hexagonal close packed (hcp) magnesium alloys because they provide grains with a means of straining along their c-axes, which the more prevalent slip modes (e.g., basal slip of <a> type dislocations) fail to do [1]. Unlike dislocation slip, twinning is a unidirectional deformation mechanism. Depending on the c/a ratio, twinning modes in hcp metals are distinguished by their ability to produce either tensile or compressive strain along the crystallographic c-axis (but not both) [2]. The dominant twinning mode in most hcp metals, including magnesium, involves shear on $\{10.2\}$ planes in $\langle 10.\bar{1} \rangle$ directions. In the case of magnesium, this is a tensile twin, since c/a ratio for magnesium is $1.62 < \sqrt{3}$.

Wrought magnesium alloys typically possess a strong texture and, lately, establishing a quantitative connection between the texture and the plastic anisotropy of magnesium alloys has been the subject of significant investigation [3, 4]. The typical deformation textures are such that the tensile twinning mode is activated by compression along the prior working direction, e.g. parallel to the extrusion axis, and inactive during tension along the same axis. This texture places the grains in unfavorable orientations for the dominant basal dislocation slip mode in both tension and compression. Thus, the unidirectional nature of deformation twinning results in the strength asymmetry (high tensile and low compressive strength) frequently observed in wrought magnesium products [5]. As the texture gets stronger, the polarity of the twinning mechanism magnifies the anisotropy of the hexagonal crystal.

The effect of twinning on the mechanical response of Mg sheet during strain path changes has only begun to be investigated [6]. In the present research, effect of load/strain reversals on twinning is explored. The reversibility of twinning is investigated by directly measuring the characteristic texture which develops during tensile and compressive deformation.

Experimental Method

All rights reserved. No part of contents of this paper may be reproduced or transmitted in any form or by any means without the written permission of the publisher: Trans Tech Publications Ltd, Switzerland, www.ttp.net. (ID: 128.165.83.86-20/11/06,17:06:29)

Material: An extruded bar of the most common magnesium alloy AZ31B was used for the cyclic loading tests. AZ31B has a nominal composition of 3 wt. % Al and 1 wt. % Zn, with restrictions on the transition metal impurities Fe, Ni, and Cu in order to improve the corrosion resistance of the alloy. The hot working results in a grain size of roughly 10 μm. The as-extruded texture has been reported in recent publications [7]. The as-extruded texture is symmetric about the extrusion axis, with the vast majority of basal poles normal to and the prism poles parallel with the extrusion axis.

In-situ Neutron Diffraction: In-situ uniaxial deformation on the Spectrometer for Materials Research at Temperature and Stress (SMARTS) [8] and texture measurements on the High-Pressure-Preferred Orientation (HIPPO) [9] have been discussed extensively in the literature, so only a brief discussion highlighting the changes necessary for cyclic tension-compression measurements on SMARTS will be presented here. A purpose built horizontal load frame was used to load the samples in tension and compression with the load axis at 45° from the incident beam. Detectors on either side of the specimen simultaneously record data with diffraction vectors, parallel $Q_{\parallel}$ (-90º) and transverse $Q_{\perp}$ (+90º), to the applied load [10-12]. The sample was designed according to ASTM standard E606-92 and the grips were similar in principle, but slightly different in detail, from that shown in figure 3c of that standard. An extensometer spanning the irradiated region recorded the macroscopic strain during the entire test.

The diffraction geometry of SMARTS, defined by the position of the detector banks at ±90° and the placement of the load axis at 45°, coupled with the as-extruded texture are advantageous for the study of deformation twinning [12]. Initially, diffracted intensity from the basal (00.2) poles is absent in the $Q_{\parallel}$ detector and strong in the $Q_{\perp}$ detector. Conversely, prism pole (e.g., (10.0) and (11.0) intensity is initially strong in the $Q_{\parallel}$ detector and weak (although not completely absent) in the $Q_{\perp}$ detector. During a twinning event, the symmetry axis of the crystal structure rotates 180° about the twin plane normal [13, 14] resulting in a 86.6° reorientation of the basal pole from perpendicular to the stress axis to nearly parallel. Given the sample orientation, this nearly 90° reorientation of the basal pole during twinning results in a transfer of (00.2) diffraction intensity from the $Q_{\perp}$ to the $Q_{\parallel}$ detector. Similarly, the prism plane diffraction intensity concomitantly transfers from the $Q_{\parallel}$ to the $Q_{\perp}$ detector. The transfer of intensity between the two detector banks allows for a direct measure of the twinned volume fraction, as demonstrated in previous publications [12].

Cyclic deformation was carried out *in situ* in strain control with amplitude of ±1% strain. The initial compressive deformation (first cycle) was completed in steps of -0.2% to –1% strain (strain rate) with neutron diffraction data collected for 20 minutes at each step. Similarly, diffraction data were taken at strain intervals to a maximum tensile strain of 1%. During the subsequent cyclic deformation, only select cycles were chosen for study with neutron diffraction. Diffraction data were collected at 1% strain, 0 MPa stress, 0 strain, -1% strain, 0 MPa stress, 0 strain and 1% strain within cycles 2, 5, 9, 13, 31, 51, 76, 101, and 251. Between these cycles the sample was cyclically deformed at a frequency of 1 Hz. Thus, it must be noted that the strain rate during the cycles in which diffraction was recorded was significantly different than the intervening cycles. The sample fractured during the 436th cycle.

Data Analysis: Determination of the crystallographic texture from diffraction data collected on HIPPO using the spherical harmonics expansion within the General Structure Analysis Software (GSAS) is now well established [15], especially for the case of relatively smoothly varying textures. In contrast, the two diffraction patterns collected simultaneously on SMARTS are insufficient to determine the complete ODF. However, the Time of Flight (TOF) technique inherently lends itself to determining the inverse pole figure along the direction of the diffraction vector. Roughly 25 independent diffraction peaks are resolvable in a single diffraction pattern collected with a common

diffraction vector. The relative pole density of several grain orientations spread across the irreducible stereographic triangle can be determined from the intensity of their respective diffraction peaks.

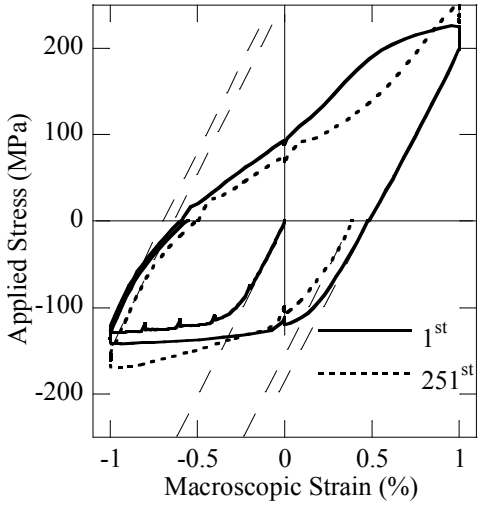

Figure 1. Flow curve on first and 251st cycle. Dashed lines represent the elastic modulus.

Results

Macroscopic Deformation: For clarity, Figure 1 shows only the first and last (251st) flow curves measured before the sample fractured. The dashed lines represent the elastic modulus of the material (42 GPa), translated when necessary to be easily comparable to the data. The initial compressive deformation is consistent with that shown in reference [16]. Deviations from linearity are first observed a –76 MPa, with the 0.2% limit at –120 MPa. Very little hardening is observed initially due to the activation of deformation twinning and the maximum compressive strain of –1% is reached at –127 MPa. On reversal, the stress/strain curve noticeably departs from linearity at –52 MPa, before returning to the macroscopic unstressed condition. This Bauschinger-type recovery during unload is unexpected as it was not observed in previous studies to -5% deformation [16]. The 0.2% strain limit is reached at 30 MPa on the tensile half of the first cycle. The hardening is steeper during tension, but the sigmoidal shape characteristic of deformation twinning is still evident. During unloading from the maximum tensile strain of 1% (225 MPa), the stress/strain curve is linear until roughly –73MPa; the strain recovery evident on unloading from compression was not seen following tensile deformation.

The 0.2% strain limit of the second compressive cycle was –120 MPa, comparable to the first compressive cycle. Also, the hardening and unloading of the second cycle were similar to the first with –1% strain (-1.5 % from crossing 0 MPa) reached at –140 MPa and the non-liner strain recovery initiating at –65 MPa during unloading. In contrast, the shape of the flow curve on the compressive side of the 251st cycle, the last before failure, is significantly different. The initial deviation from linearity occurs at a lower stress, -53 MPa, and the hardening is much steeper. The stress at the maximum compressive strain of –1% was –170MPa. Once again significant strain recovery is observed during unloading, starting at about –60 MPa. The flow curve on the final tensile cycle is similar to the first, except the plateau region seems a bit larger, and the second yield point was not reached by the maximum strain.

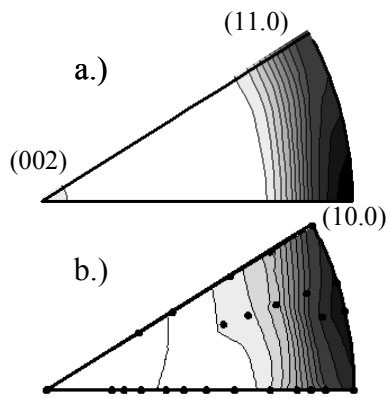

Figure 2. As-extruded inverse pole figures along the extrusion direction measured using a.) HIPPO (full texture analysis) and, b.) SMARTS diffractometers. Contours are drawn from 0 to 4 multiples of random distribution at intervals of 0.25.

Texture Development: Figure 2 compares the inverse pole figures along the extrusion direction measured on the as-extruded material using HIPPO and the corresponding analysis of the complete orientation distribution function and determined on SMARTS on the same scale. The dots on the SMARTS inverse pole figure indicate the location of the grain orientations analyzed to obtain the contours; the coverage is not bad. Clearly even 25 points on the inverse pole figure is insufficient for accurate quantitative determination of the entire inverse pole figure, but it allows for qualitative observations on the

development of the texture within a single deformation cycle and at a single point, say at –1% strain, across multiple cycles. The agreement is not exact, and inverse pole figures determined *ex situ* on HIPPO are considered more accurate, but again, the inverse pole figures determined on SMARTS appear close enough to make qualitative observations.

Figure 3 shows the inverse pole figures in the extrusion (straining) direction measured at the conditions of maximum compression and tension strain of the first, second, and 251st cycles. Initially, there is primarily prism pole density along the extrusion axis; very little basal pole density is present (Fig. 2). After the first –1% of deformation, a significant fraction of the microstructure has reoriented due to the activity of deformation twinning, manifested by the increase basal pole density in the straining direction. Unloading and reloading to 1% tensile strain reverses the build up of basal pole density in the straining direction. Indeed, the texture after the first tensile loading is not significantly different from the initial texture (compare Figs. 2b and 3b).

The basal density aligned with the compression axis, which is indicative of twinning, is higher after the second deformation to –1% than the first because the material was effectively deformed more, starting at nearly tensile 1% strain at zero load instead of 0 (see Fig. 3c). Similar to the first deformation to the tensile maximum strain, the texture is not significantly different from the as-extruded texture when 1% strain is reached a second time (Fig. 3d). After 251 cycles, the inverse pole figure after –1% compressive strain shows significantly more basal pole density (2 contours or 0.5 MRD) than the same point of the second cycle (compare Figs. 3c and 3e). Correspondingly, there is slightly less (11.0) prism pole density aligned with the stress axis after the 251st compressive cycle than the second, although it is difficult to see on the contour plots due to the coarseness of the contours. Similarly, the (11.0) prism pole density is also reduced after the 251st tensile cycle relative to the first and second cycles and there is some residual basal pole density although, again, it is not evident on the contour plots. The inverse pole figures shown in figure 3 represent snap shots of the texture at several stages of the cyclic deformation and are quite illustrative of the crystallographic response of the material, but are less useful for quantitative discussion of the development of the texture.

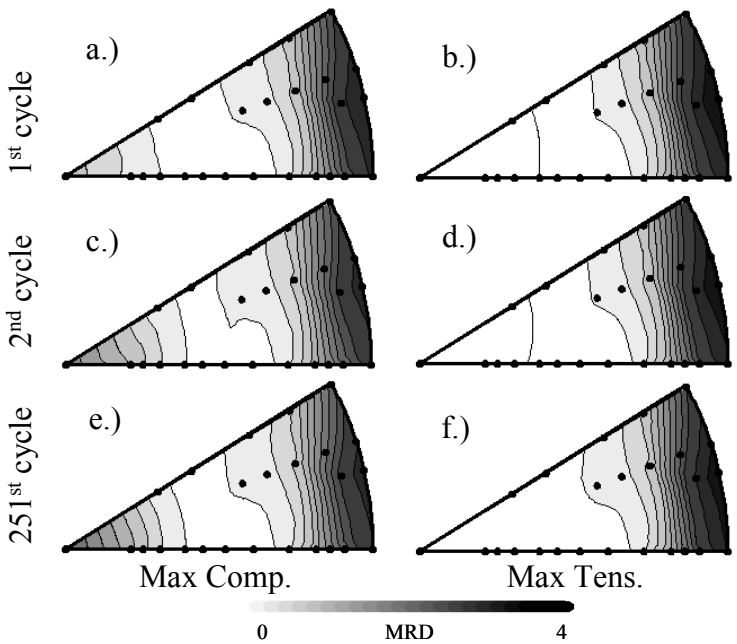

Figure 3. Inverse pole figures measured along the extrusion/loading direction of extruded magnesium under conditions of a.) first max compression, b.) first max tension, c.) second max compression, d.) second max tension, and e.) last (251st) max compression, f.) last max tension. Same scale as Figure 2.

Figures 4a and b show the integrated diffracted intensities of the basal (00.2) peak and three of the prism ((10.0), (11.0), and (21.0)) peaks as a function of run number (which is used for experimental bookkeeping to identify diffraction data) during the cycling. The actual cycle number is also noted. In order to facilitate comparison on the same plot, the prism peak intensities are normalized to 1 at the initial measurement (and offset from each other for clarity) and the basal peak intensity is normalized to one at its maximum value. The short

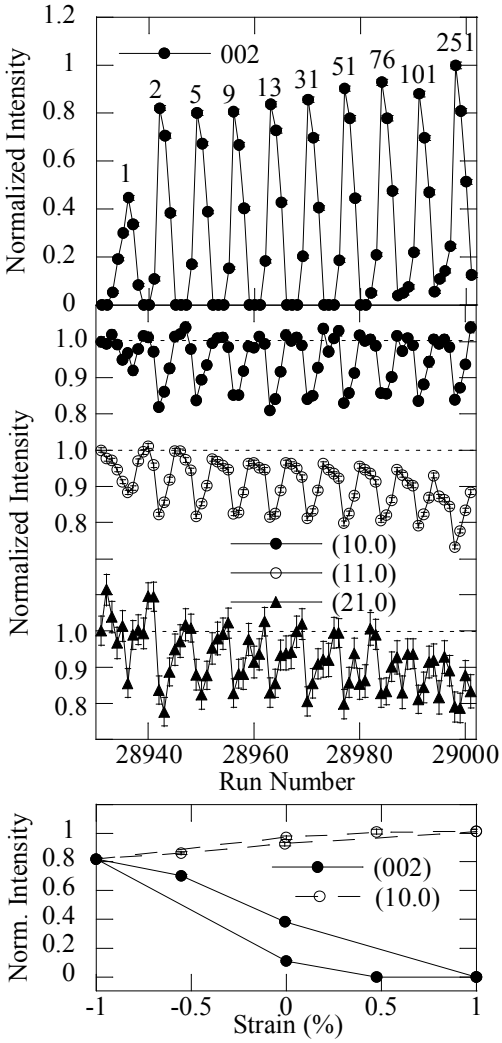

Figure 4. Diffracted peak intensity variation of a.) basal and b.) prism poles throughout cycling and c.) within a single representative cycle.

wavelength oscillations represent the texture development within one cycle; the maxima in the basal pole intensity occur at maximum compression, the minima at tension and vice versa for the prism poles. Recall that several cycles were run at 1 Hz between cycles in which diffraction data was recorded, so only selected cycles are shown in figure 4.

To highlight the development of the texture during a single representative deformation cycle, the (00.2) and (10.0) integrated peak intensities during the second deformation cycle (starting at 1% tensile strain) are shown in figure 4c. At the initial point, the texture is equivalent to the as-extruded texture to within experimental uncertainty. No change in diffracted intensity indicative of texture development is observed during unloading from maximum tension to 0 MPa (0.5% tensile strain). A strong increase in (00.2) peak intensity, and concomitant decrease in (10.0) intensity, is observed during subsequent compression. In contrast, during unloading from the maximum compressive strain, the (00.2) peak intensity decreases significantly, falling to half its value in the unloaded condition. As shown in figure 3, at the end of the second cycle the texture is again similar to the original.

The complete recovery of the texture on return to the maximum tensile stress does not continue indefinitely. Figures 4a and b clearly show that by the fifth cycle, the recovery of (11.0) peak intensity at maximum tension is incomplete and, subsequently, the loss of intensity increases monotonically with increased cycles. Similarly, the (11.0) intensity at maximum compression also decreases with increased cycles. The (21.0) intensity follows a similar trend, but appears to start significantly later, after roughly 76 cycles. The (21.0) peak initially has lower raw intensity (few neutron counts) making the data noisier, which makes the initiation point more difficult to ascertain. Interestingly, the (10.0) intensity is completely recovered by tensile loading through the last cycle measured before fracture. The (00.2) intensity at maximum compression increases notably after roughly 13 cycles and continues increasing throughout cycling, corresponding to the loss of prism pole intensity. Residual basal pole intensity at maximum tension is measurable after the 76th cycle. Notably, the (00.2) peak is present at maximum tension in earlier cycles, but the peak is too diminutive to fit accurately.

In the interest of brevity, the behavior of the peak intensities in the transverse direction is not discussed here. It suffices to say that the trends in the intensities observed in the transverse detector banks are consistent with those described in the straining direction.

Discussion

Twinning and detwinning during cyclic deformation: As described in the introduction, the polar nature of deformation twinning and the typical texture of magnesium extrusions result in deformation

twinning being active during compressive deformation along the extrusion direction (normal to the basal poles) but not during tensile deformation in the same orientation [17]. The discrete crystallographic reorientation associated with twinning results in the radical texture development [12, 18] observed during the initial compressive deformation shown in the inverse pole figures (Fig. 3).

The initial as-extruded texture is not favorable for twinning in tension. However, the grains that have twinned during compression are in optimal orientation to twin again (or de-twin) during subsequent tensile straining since the basal poles are parallel to the tensile axis after the initial compressive strainning. The reversal of the texture that developed during compression is a clear indication of de-twinning during tension. Lou et al. [6] have also reported de-twinning during cyclic deformation.

Clearly, the ability to twin and de-twin within a compression-tension cycle is maintained through at least 250 cycles. However, the capacity to reversibly switch the texture reduces with increased cycling. After several cycles, some residual twins are observed even at the maximum tensile strain. Specifically, grains whose (11.0) and (21.0) poles were originally parallel to the extrusion direction fail to de-twin after roughly 5 and 76 cycles, respectively. In contrast, (10.0) grains twin and de-twin reversibly throughout the duration of the experiment (251 cycles). While it is not generally accepted that deformation twinning is controlled by a resolved shear stress, it is informative to consider the Schmidt factor, $m = \cos\lambda\cos\chi$ (where λ and χ represent the angle between the stress axis and the twin plane normal and twin direction, respectively) of the different prism grain orientations. Grains whose (10.0), (21.0), and (11.0) poles are parallel to the load axis have a maximum Schmidt factors of m = 0.49, 0.45, and 0.37, respectively. Thus, the ability to continuously twin and de-twin during cyclic deformation is at least correlated to the resolved shear stress for twinning within the grain.

The hardening rate in compression also increases concurrent with the observed increase in residual twins. Presumably, the residual twins result in hardening in the material, with twin boundaries possibly acting as barrier to dislocation motion.

Strain and texture recovery during unload: The macroscopic flow curve (Fig. 1) shows significant strain recovery during unloading from –1% strain, but not during unloading from 1% strain. Similarly, notable texture recovery is observed during unload from –1% strain, but not from 1% strain.

Neither strain nor texture recovery were observed during unloading in previous studies of deformation twinning in rolled and extruded magnesium to compressive strains greater than –5% [12, 16]. *In-situ* measurements of the strain state of the newly formed twins show that when they first form, the twins are in a tensile stress state parallel to the compression direction relative to the surrounding grains, that is to say, twins form with a tensile intergranular stress along the basal pole [12, 16]. The newly formed twins are in a plastically hard orientation (basal poles parallel to the straining direction) and quickly accumulate elastic strain and develop compressive intergranular strain by -5% deformation. Thus, when unloading from small macroscopic strains, i.e. –1%, the twins de-twin very early due to the tensile intergranular stress they feel from surrounding grains, but when unloading from larger strains, -5% or larger, the compressive intergranular stress prevents them from recovering early. At this point, we do not have enough information regarding the stress state of the grains after reaching the maximum tensile strain to understand the asymmetry observed during unloading.

Conclusions

In situ neutron diffraction measurements were completed during compression-tension cyclic loading of extruded magnesium alloy AZ31B to amplitude of ±1% strain for 251 cycles. The diffraction

geometry coupled with the as-extruded texture result in clean separation of the (00.2) peak intensity (basal poles) in the $Q_{\perp}$ detector and (10.0), (11.0), and (21.0) peak intensity (prism poles) in the $Q_{\parallel}$ detector. Repeatable flipping of the crystallographic texture associated with deformation twinning and de-twinning is observed throughout the cycling. The capacity to reverse twins formed on compression during subsequent tensile deformation reduces with increase cycling. In particular, grains whose (11.0) and (21.0) poles are initially parallel to the extrusion axis fail to de-twin after a few cycles. Concurrently, the hardening of the material increases with increased cycle, presumably due to the presence of the residual twins.

Acknowledgements

Research sponsored by Los Alamos National Laboratory under grant number W-7405-ENG-36. The Manuel Lujan Jr. Neutron Scattering Center is a national user facility funded in part by the U.S. DOE.

References

1. Kocks, U.F. and Westlake, D.G., Trans Metall Soc 1967, 239(7), p. 1107-&.
2. Yoo, M., Met Trans A, 1981, 12(3), p. 409-418.
3. Agnew, S., Tome, C., Brown, D., Holden, T., and Vogel, S., Scripta Mat, 2003, 48(8), p. 1003-1008.
4. Barnett, M.R., Keshavarz, Z., Beer, A.G., and Atwell, D., Acta Mat, 2004, 52(17), p. 5093-5103.
5. Ball, E.A. and Prangnell, P.B., Scripta Mat, 1994, 31(2), p. 111-116.
6. Lou, X.Y., Li, M., Boger, R.K., Agnew, S.R., and Wagoner, R.H., To appear in Int J Plasticity, 2006.
7. Agnew, S.R., Horton, J.A., Lillo, T.M., and Brown, D.W., Scripta Mat, 2004, 50(3), p. 377-381.
8. Bourke, M., Dunand, D., and Ustundag, E., App Phys A, 2002, A74, p. S1707.
9. Wenk, H., Lutterotti, L., and Vogel, S., Nuclear Instruments & Methods In Physics Research Section A-Accelerators Spectrometers Detectors And Associated Equipment, 2003, 515(3), p. 575-588.
10. Shi, N., Bourke, M.A.M., Roberts, J.A., and Allison, J.E., Met Trans A, 1997, 28(#12), p. 2741-2753.
11. Bourke, M.A.M., Goldstone, J.A., and Holden, T.M., in *Measurement of Residual and Applied Stress Using Neutron Diffraction*, M.T. Hutchings and A.D. Krawitz, Editors. 1992, Kluwer Academic Publishers: The Netherlands. p. 369-382.
12. Brown, D.W., Agnew, S.R., Bourke, M.A.M., Holden, T.M., Vogel, S.C*., et al.*, *Mat Sci Eng A*, 2005, 399(1-2), p. 1-12.
13. Cahn, R.W., Acta Metall, 1953, 1, p. 50-74.
14. Reed-Hill, R.E. and Abbaschian, R., in *Physical Metallurgy Principles*. 3 ed. 1994, Boston, MA 02116-4324: PWS Publishing Company.
15. Von Dreele, R.B., J Appl Cryst, 1997, 30, p. 517-525.
16. Brown, D.W., Agnew, S.R., Abeln, S.P., Blumenthal, W.R., Bourke, M.A.M., et al., Mat Sci Forum, 495-497, p. 1037-1042.
17. Agnew, S.R., Brown, D.W., and Tome, C.N., submitted to Acta Mat, 2006.
18. Brown, D.W., Abeln, S.P., Blumenthal, W.R., Bourke, M.A.M., Mataya, M.C., et al., Met Trans A, 2005, 36A(4), p. 929-939.